Examples and Counterexamples 2 (2022) 100047

Contents lists available at ScienceDirect

Examples and Counterexamples

journal homepage: www.elsevier.com/locate/exco

On the relation of Gamma-convergence parameters for pressure-driven quasi-static phase-field fracture

Leon Kolditz *, Katrin Mang

Leibniz Universität Hannover, Institute for Applied Mathematics, Welfengarten 1, 30167 Hannover, Germany

ARTICLE INFO

Keywords:
Γ-convergence
Phase-field
Bulk regularization
Pressure-driven fracture
Error analysis

ABSTRACT

The proof of Γ-convergence builds the base of the well-known Ambrosio–Tortorelli functional leading to an energy functional for quasi-static phase-field fracture problems. Three parameters in a monolithic quasi-static phase-field fracture model are very relevant for the quality of the results: the length-scale ϵ, the regularization parameter κ to avoid ill-posedness of the system and the discretization parameter h. The work on hand presents numerical results considering a pressure-driven cavity in 2d with two quantities of interest, the crack opening displacement and the total crack volume. The focus will be to discuss the assumptions of Γ-convergence which demand: $h = o(\kappa)$ and $\kappa = o(\epsilon)$ and $\epsilon \to 0$. An error analysis of the chosen quantities of interest allows to identify a proper setting for the three mentioned model parameters.

1. Introduction

Phase-field fracture modelling is a popular approach to simulate crack propagation in brittle materials. In the context of a quasi-static phase-field fracture model based on the Ambrosio–Tortorelli functional [1,2], we have a regularization parameter $0 < \kappa \ll 1$ which regularizes the bulk energy [3]. This parameter should be as small as possible to avoid over-estimation of the bulk energy (resulting in an under-estimation of the surface crack energy). In practice, it means: the larger the value of κ, the slower the crack will grow. In [4], the model parameter κ is introduced to prevent the positive part of the elastic energy density from disappearing when the phase-field is equal to zero, which has been observed to improve computational robustness in the quasi-static simulations presented by Miehe et al. [5]. In the frame of this work, we observe κ similarly to [4] as a purely numerical quantity. Bellettini and Coscia [6] showed in 1994, that the AT2 functional Γ-converges to the Mumford and Shah functional [7] for $\epsilon \to 0$ and $\frac{\kappa}{\epsilon}$ tends to zero for $\epsilon \to 0$, where ϵ is the approximative crack width. In a mechanical context it is written, that Bellettini and Coscia [6] proved the Γ-convergence for $\kappa \to 0$, $\epsilon \to 0$ and $h \to 0$ with $\kappa \ll \epsilon$ and $h \ll \epsilon$, where h is the discretization parameter. This does not directly postulate that $h \ll \kappa$.

In 1999, Bourdin et al. [8] presented the Γ-convergence of the discretized Mumford and Shah functional [7] for image segmentation with the assumption $h \ll \kappa \ll \epsilon$, because then $min(E_{\epsilon,h})$ converges to $min(F)$ as $\epsilon \to 0$. In first numerical results on images, the parameters are chosen such that $h \ll \kappa \ll \epsilon$. Bourdin in 2000 [9] presented a phase-field fracture model based on the Ambrosio Totorelli AT2 functional [1,2] with the restrictions $h \ll \epsilon$ and $h \ll \kappa$. Borden in 2012 [10] determined $\kappa = 0$ for a dynamic phase-field fracture model and argues that a positive small κ is not necessary for the Γ-convergence powered by Braides 1998 [11]. Later in 2015 and 2017, the possible discrepancy between theoretical and numerical results with respect to the Γ-convergence are discussed [12,13].

The following work is structured as follows: in Section 2 the problem formulation of a pressure-driven phase-field fracture model is derived. In Section 3, the Γ-convergence is defined for the introduced energy functional. In Section 4, a detailed series of numerical results is presented and discussed to understand the conducted error analysis for a reliable setting for κ, ϵ and h.

2. Notation and problem formulation

We start with the basic notation and problem formulation for phase-field fracture similar to [14]. Throughout this work, we use the Landau notation for evaluating the limit behaviour of the considered parameters:

$$k = o(f) \iff \frac{k}{f} \to 0.$$

It means that k tends to 0 faster than f.

The scalar-valued L^2-product is denoted by

$$(x, y) := \int_\Omega x \cdot y \, d\Omega,$$

* Corresponding author.
E-mail addresses: leon.kolditz@stud.uni-hannover.de (L. Kolditz), mang@ifam.uni-hannover.de (K. Mang).

https://doi.org/10.1016/j.exco.2022.100047
Received 11 June 2021; Received in revised form 24 October 2021; Accepted 11 January 2022

whereas the vector-valued L^2-product is described by

$$(X,Y) := \int_\Omega X : Y \, d\Omega,$$

with the Frobenius product $X : Y$ of two vectors X, Y. The domain $\Omega \in \mathbb{R}^d$ ($d = 2$ for the later proposed example) is an open, connected and bounded set. The crack C is a lower-dimensional set contained in Ω.

In the following, the energy functional given by Francfort and Marigo [15] is provided, which describes the energy of elastic material under stress. The functional is given by

$$\begin{aligned} E(u,C) = &\frac{1}{2}\int_\Omega \sigma(u) : e(u)\, dx \\ &- \int_C \tau \cdot u \, ds + G_C \mathcal{H}^{d-1}(C), \end{aligned} \tag{1}$$

where $u : \Omega \to \mathbb{R}^d$ is a vector-valued displacement function and $\sigma = \sigma(u)$, the classical stress tensor of linearized elasticity is defined as

$$\sigma(u) := 2\mu e(u) + \lambda \operatorname{tr}(e(u)) I,$$

with the Lamé coefficients $\mu, \lambda > 0$ and the identity matrix I. The symmetric strain tensor $e(u)$ is given by

$$e(u) := \frac{1}{2}(\nabla u + \nabla u^T).$$

The energy functional $E(C,u)$ can be split into three terms: a bulk energy term, a traction term and a crack energy term. Traction forces are denoted by τ. The crack energy is described by $G_C \mathcal{H}^{d-1}(C)$, where $G_C > 0$ is the critical energy release rate determined by the considered material and $\mathcal{H}^{d-1}$ is the $d-1$ dimensional Hausdorff-measure.

Using $E(u,C)$, adding a pressure term, the introduced notation for the L^2-product, and following [9], the functional reads as

$$\begin{aligned} E_\epsilon(u,\varphi) = &\frac{1}{2}(((1-\kappa)\varphi^2 + \kappa)\sigma(u), e(u)) + (\varphi^2 p, \operatorname{div} u) \\ &+ G_C \int_\Omega \frac{1}{2\epsilon}(1-\varphi)^2 + \frac{\epsilon}{2}|\nabla\varphi|^2 \, dx, \end{aligned} \tag{2}$$

where $p : \Omega \to \mathbb{R}$ is a given scalar-valued pressure field. Here, the surface energy term (the third term in Eq. (1)) was replaced by an Ambrosio–Tortorelli approximation.

The regularized problem, which is later solved, is then given by

$$\min E_\epsilon(u,\varphi) \text{ such that } \partial_t \varphi \le 0.$$

The inequality constraint represents the crack irreversibility. For deriving an incremental version, the constraint can be discretized in time via classical finite difference time discretization. Based on [3], the function spaces

$$\begin{aligned} V &:= H_0^1(\Omega), \\ W_{\text{in}} &:= \{w \in H^1(\Omega) | w \le \varphi^{n-1} \le 1 \text{ a.e. on } \Omega\}, \\ W &:= H^1(\Omega), \end{aligned}$$

lead to the following weak problem formulation:

Find $(u,\varphi) \in V \times W$ with

$$\left(((1-\kappa)\varphi^2 + \kappa)\,\sigma(u), e(w)\right) + \left(\varphi^2 p, \operatorname{div} w\right) = 0, \ \forall\, w \in V,$$

and

$$\begin{aligned} &(1-\kappa)(\varphi\sigma(u) : e(u), \psi - \varphi) + 2(\varphi p \operatorname{div} u, \psi - \varphi) \\ &\quad + G_C\left(-\frac{1}{\epsilon}(1-\varphi, \psi-\varphi) + \epsilon(\nabla\varphi, \nabla(\psi-\varphi))\right) \\ &\quad \ge 0, \ \forall\, \psi \in W_{\text{in}} \cap L^\infty(\Omega). \end{aligned}$$

3. Statement of Γ- convergence

The introduced energy functional $E_\epsilon(u,\varphi)$ in Eq. (2) is based on Griffith's idea of fracture [16]. Griffith's law was the starting point for developing the functional $E(u,C)$. Thus, we need to ensure that we solve the same problem when minimizing $E_\epsilon(u,\varphi)$ as when seeking for the minimum of $E(u,C)$. This is where Γ-convergence comes into play. From Γ-convergence it follows that a minimizer of $E_\epsilon(u,\varphi)$ converges to a minimizer of E as $\epsilon \to 0$, see [17,18] for further details. The definition of Γ-convergence in the following is based on [11,17].

Definition 3.1. For a given sequence of functions $(f_j) : X \to \bar{\mathbb{R}}$ and a function $f_\infty : X \to \bar{\mathbb{R}}$, the sequence (f_j) Γ-converges in X to f_∞, if for all $x \in X$ it holds

(i) for every sequence (x_j) converging to x

$$f_\infty(x) \le \liminf_{j\to\infty} f_j(x_j) \qquad \text{(lim inf inequality)},$$

(ii) there exists a sequence (x_j) converging to x such that

$$f_\infty(x) \ge \limsup_{j\to\infty} f_j(x_j) \qquad \text{(lim sup inequality)}.$$

The function f_∞ is called the Γ-limit of (f_j) and we write $f_\infty = \Gamma\text{-}\lim_j f_j$.

The following theorem states the Γ-convergence of the functional E_ϵ to E:

Theorem 3.2. *The regularized functional $G_j : L^1(\Omega) \times L^1(\Omega) \to \mathbb{R}$, defined by*

$$G_j(u_j,\varphi_j) = \begin{cases} E_{\epsilon_j}(u_j,\varphi_j) & \text{if } (u_j,\varphi_j) \in H^1(\Omega) \times W_{in}, \\ +\infty & \text{otherwise} \end{cases}$$

Γ-converges, as

$$\epsilon_j \to 0^+ \text{ for } j \to \infty \text{ and } \kappa = o(\epsilon_j),$$

to the functional $G : L^1(\Omega) \times L^1(\Omega) \to \mathbb{R}$, given by

$$G(u,\varphi) = \begin{cases} E_T(u) & \text{if } \varphi = 1 \text{ a.e. and } u \in PH^1(\Omega), \\ +\infty & \text{otherwise}, \end{cases}$$

where $PH^1(\Omega)$ is the space of functions, which are piecewise H^1-functions on Ω. Furthermore, if (u_j,φ_j) is a minimizer of G_j, then (u_j,φ_j) (possibly a subsequence) converges to a minimizer of G.

For the proof of the latter theorem for the pressure-driven phase-field fracture functional we refer to [19] based on the works of Braides [11,17].

Remark 3.3. Note that the Γ-convergence property also holds true for the discretized problem under the assumption that $h = o(\epsilon_j)$, where h is the spatial discretization parameter. Further, κ is necessary to ensure that the stress term does not vanish when $\varphi = 0$. This in turn means, κ must be small enough. Otherwise the bulk energy would be overestimated. It is handled by assuming $\kappa = o(\epsilon_j)$.

4. Numerical studies on Γ - convergence

In this section, numerical results are given to justify the impact of the regularization parameter κ for a pressure-driven cavity while satisfying the assumptions on Γ-convergence and giving promising results for the considered quantities of interest. We use H^1-conforming finite elements on quadrilaterals (2D). Specifically, we use bilinear elements Q_c^1 [20] for both, the displacements and the phase-field variable. In accordance with Heister et al. [3], a monolithic approach with an extrapolation of the phase-field variable in the displacement equation is used. To treat the variational inequality, we follow [3] with a primal–dual active set method. The used code for all numerical tests is derived from an open-source project by Heister and Wick [21] based on deal.II [22].

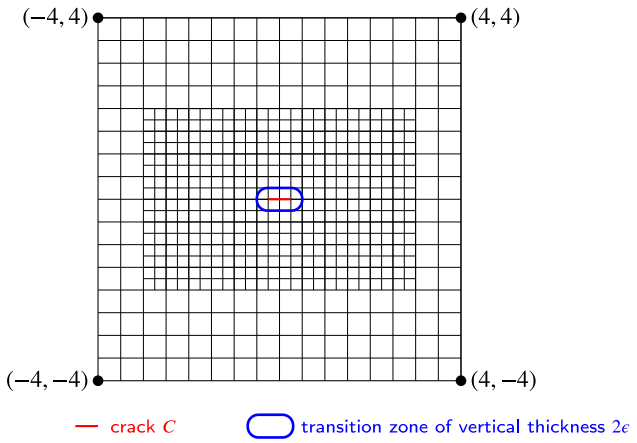

Fig. 1. Zoom-in of the whole domain $\Omega = (-10, 10)^2$ to the pre-refined crack zone in $[-4, 4] \times [-4, 4]$ with 2 global refinement steps and 1 local refinement step.

4.1. A pressure-driven cavity in 2d

We consider a stationary benchmark test [14], where constant pressure is applied in the inner of a pre-existing crack in the middle of a domain. This test setup is motivated by [23,24]. For the time being we restrict ourselves to a 1d fracture C on a 2d domain $\Omega = (-10, 10)^2$ as depicted in Fig. 1. The fracture is centered horizontally within Ω and has a constant half crack length $l_0 = 0.25$ and varying width. Specifically, the crack width corresponds to $2h$, where h is the minimal cell diameter of the mesh. The mesh is pre-refined geometrically in the crack zone, such that the area, where $\varphi < 0.999$, is covered with the smallest mesh size. The driving force is given by a constant pressure $p = 10^{-3}$ Pa in the inner crack. An overview of the parameter setting is given in Table 1.

4.2. Quantities of interest

For the evaluation of the numerical results for the described benchmark test, two certain quantities of interest will be discussed: the crack opening displacement (COD) and the total crack volume (TCV). The COD is defined on an infinite domain as

$$\mathrm{COD}(x) := [u \cdot n](x) \approx \int_{-\infty}^{\infty} u(x, y) \cdot \nabla \varphi(x, y)\, dy.$$

In the numerical tests, the displacement jumps are computed on the finite domain $\Omega = (-10, 10)^2$. The maximum of COD is reached in $x = 0$ and thus given by

$$\mathrm{COD}_{\max} := [u \cdot n](0) \approx \int_{-\infty}^{\infty} u(0, y) \cdot \nabla \varphi(0, y)\, dy.$$

The analytical solution (cf. [24]) is given by

$$\mathrm{COD}_{\mathrm{ref}} = 2\frac{pl}{E'}\left(1 - \frac{x^2}{l_0^2}\right)^{\frac{1}{2}},$$

where $E' := \frac{E}{1-\nu^2}$. The TCV can be computed numerically with

$$\mathrm{TCV} = \int_{\Omega} u(x, y) \cdot \nabla \varphi(x, y) d(x, y).$$

The analytical solution (cf. [24]) is given by

$$\mathrm{TCV}_{\mathrm{ref}} = \frac{2\pi p l_0^2}{E'},$$

where $E' := \frac{E}{1-\nu^2}$ and E is the Young's modulus and ν is the Poisson ratio.

Table 1
The setting of the material and numerical parameters used for the numerical tests in Section 4.

Parameter	Definition	Value
Ω	Domain	$(-10, 10)^2$
h	Diagonal cell diameter	test-dependent
l_0	Half crack length	0.25
G_C	Material toughness	1.0
E	Young's modulus	1.0
μ	Lamé parameter	0.42
λ	Lamé parameter	0.28
ν	Poisson's ratio	0.2
p	Applied pressure	10^{-3}
TOL_t	Tolerance time step loop	10^{-5}
ϵ	Bandwidth of the initial crack	test-dependent
κ	Regularization parameter	test-dependent

Table 2
Results of maximal crack opening displacement ($\mathrm{COD}_{\max}$), total crack volume (TCV) and number of degrees of freedom (#dof) for different mesh sizes h and the relations of Case 1 in Eq. (4) compared to the reference values of Sneddon and Lowengrub.

h	$\mathrm{COD}_{\max}$	TCV	#dof
0.0221	0.000286517	0.000313325	43,605
0.0110	0.000274623	0.000276284	100,089
0.0055	0.000267051	0.000253393	176,709
0.0027	0.000263680	0.000239692	628,533
Ref. [24]	0.000480000	0.000376991	–

4.3. Numerical results: fails

As stated in the latter theorem, Γ-convergence requires a specific choice of the regularization parameters κ and ϵ. Further, we need to choose $\epsilon > h$ in the case of low-order finite elements [25] to ensure that the mesh does not skip the crack. This leads to the following relations:

$$\kappa = o(\epsilon) \quad \text{and} \quad h = o(\epsilon), \tag{3}$$

as $\epsilon \to 0$ (which is numerically desirable, but challenging). A possible choice, similar to Case 4 in [26], is

$$\textbf{Case1}: \kappa = 0.25h^{0.5} \quad \text{and} \quad \epsilon = 0.25h^{0.25}. \tag{4}$$

This setting satisfies the Γ-convergence conditions we introduced in Eq. (3) for all $h < 0.5$ and further $h < \epsilon$ is satisfied for all $h < 0.5$.

Remark 4.1. In contrast to [19], ϵ, κ and h are not decreased proportionally, but according to the condition that κ has to tend faster to 0 than ϵ, and h faster to 0 than ϵ.

Satisfying the relations of κ and ϵ as denoted in Case 1, the numerically achieved COD values and TCV values are given in Fig. 2 and Table 2 for different minimal mesh sizes h. One can see, that with a smaller h the COD values are converging to a curve far away from the analytical solution proposed by Sneddon and Lowengrub [24] on an infinite domain.

Remark 4.2. Note that the TCV value for $h = 0.022$ is relatively close to the exact reference. This should not be misinterpreted since TCV is the integral of the COD curve and even if the exact COD is underestimated, the approximative bell curve is wider than the exact one, which results in a larger (or in this case more precise) TCV value.

To resolve the crack area, h can be assumed to be sufficiently small to give satisfactory COD and TCV values, in comparison to the literature, e.g. [27]. One possible reason for imprecise COD values may be the regularization parameter κ. To give quantitative arguments for this observation, in Table 3 an error analysis on κ for the TCV value is given.

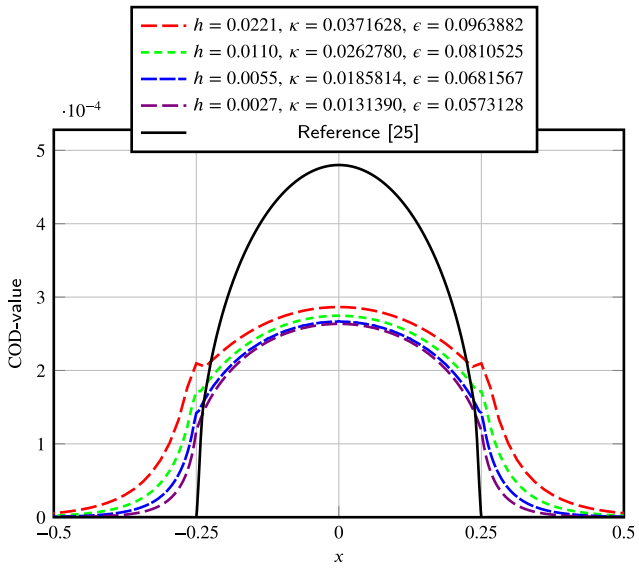

Fig. 2. Visualization of the COD-values for different h with κ and ϵ set as in Case 1 in Eq. (4). The corresponding exact TCV values and COD_{max} values are given in Table 2.

Table 3
Error in the total crack volume (TCV error) in percentage (compared to the exact TCV = 0.000376991 on an infinite domain) for different choices of κ depending on the diagonal cell diameter $h = 0.00552427$ and a fixed $\epsilon = 2h$.

κ	TCV	TCV error [%]
$h = 5.52427 \cdot 10^{-3}$	0.000239171	36.56%
$0.5h = 2.762135 \cdot 10^{-3}$	0.000290719	22.88%
$0.25h = 1.381068 \cdot 10^{-3}$	0.000330106	12.44%
$10^{-1}h = 5.52427 \cdot 10^{-4}$	0.000361447	4.12%
$10^{-2}h = 5.52427 \cdot 10^{-5}$	0.000384297	1.93%
$10^{-3}h = 5.52427 \cdot 10^{-6}$	0.000386788	2.60%
$10^{-12}h = 5.52427 \cdot 10^{-15}$	0.000387067	2.67%
Ref. [24]	0.000376991	–

4.4. Numerical results: findings

In this section possible reasons for the non-satisfactory results for two relevant quantities of interest (COD and TCV) in Section 4.3 are identified. The idea is to analyse the TCV-error for different parameter settings, especially for different values of κ. Thus, in Table 3 detailed test results are provided.

We can see, that with a tolerance of less than 4% in the error for TCV, κ should be smaller than 10^{-5}. Thus we determine

$$\kappa = 0.25h^{0.5} < 10^{-5},$$

which leads to a discretization parameter $h \approx 10^{-9}$. This would yield an unrealistic number of degrees of freedom (dof). Even if only the known crack zone $[-0.26, 0.26] \times [-0.4, 0.4]$ is refined, the problem would have a size of approximately 10^{17} dof. Thus we need to find a setting for κ, which does not violate the Γ-convergence conditions but tends to zero faster. A possible choice is given by:

$$\textbf{Case2}: \kappa = 10^{-3}h^{0.75} \quad \text{and} \quad \epsilon = 0.25h^{0.25}. \tag{5}$$

In Case 2, $h = o(\kappa)$ and $\kappa = o(\epsilon)$ is satisfied and κ is small enough for promising results of the two chosen quantities of interest with $h \approx 10^{-5}$, without exceeding the computational capacity. The behaviour of κ, ϵ and h is visualized in Fig. 3. We can see that κ is very small in Case 2, even for larger h. This is a major advantage in comparison to Case 1 since we do not need as many degrees of freedom as in Case 1. Fig. 4 provides results for the mentioned Case 2.

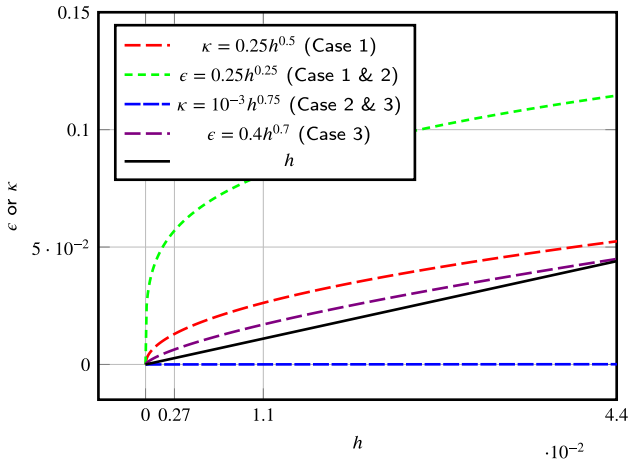

Fig. 3. Visualization of ϵ and κ set as in Case 1 and Case 2. We can see that κ is very small in Case 3 even for bigger h and ϵ satisfies $\epsilon > h$ and $h = o(\epsilon)$ for reasonable h while being very close to h.

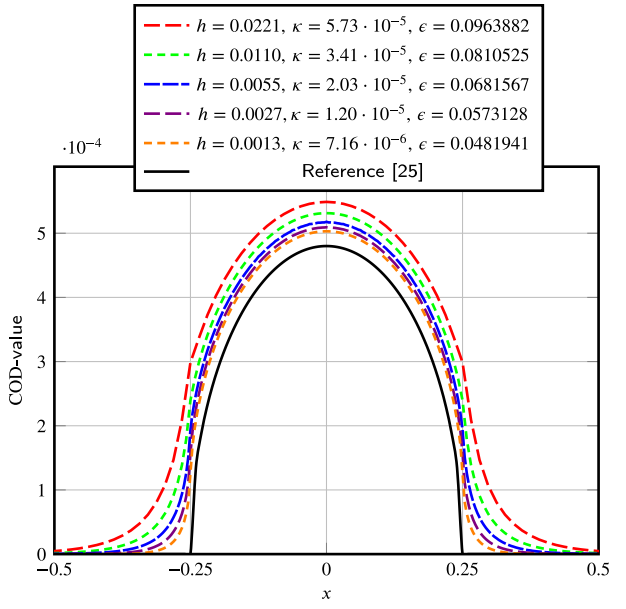

Fig. 4. Visualization of the COD values for different h with h-dependent κ and ϵ set as in Case 2 defined in Eq. (5). The corresponding exact TCV values and COD_{max} values are given in Table 4.

Table 4
Results of computations based on the relations of Case 2 defined in Eq. (5).

h	COD_{max}	TCV	# dof
0.0221	0.000548804	0.000536082	43,605
0.0110	0.000531268	0.000487890	100,089
0.0055	0.000517768	0.000456257	176,709
0.0027	0.000509288	0.000435760	628,533
0.0013	0.000503050	0.000421441	2,416,869
Ref. [24]	0.000480000	0.000376991	–

As we can see in Fig. 4 and Table 4, the results are closer to the reference values for Case 2 than for Case 1, but there is still a recognizable error.

Since κ is small enough, the error in ϵ has to be observed in the next step. An analysis on the error given in Table 5 indicates that the impact by ϵ is sufficiently small for $\epsilon \approx 3.8 \times 10^{-4}$. We expect the error to reduce even more for smaller h, which will result in smaller ϵ. For the error analysis, $\epsilon = h$ is the smallest reasonable choice since ϵ indicates

Table 5
Error in TCV in percentage (compared to the exact TCV = 0.000376991 on an infinite domain) for different choices of ϵ depending on the diagonal cell diameter $h = 0.00552427$ and a fixed $\kappa = 10^{-6}h$.

ϵ	TCV	TCV error [%]
$64h = 0.35355328$	0.000909849	141.35%
$32h = 0.17677664$	0.000608694	61.46%
$16h = 0.08838832$	0.000478809	27.00%
$8h = 0.04419416$	0.000425164	12.78%
$4h = 0.02209708$	0.000402041	6.64%
$2h = 0.01104854$	0.000390668	3.63%
$h = 0.00552427$	0.000384213	1.92%
Ref. [24]	0.000376991	–

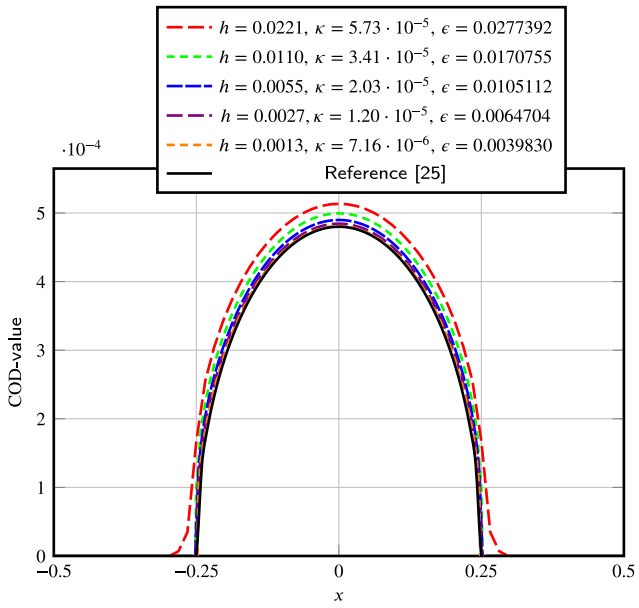

Fig. 5. Visualization of the COD values for different h with h-dependent κ and ϵ set as in Case 3 defined in Eq. (6). For the smallest h the numerical values and the reference values coincide nearly perfectly. The corresponding exact TCV values and COD_{max} values are given in Table 6.

Table 6
Numerical results of two quantities of interest (COD_{max} and TCV), and number of degrees of freedom (#dof) for different h with h-dependent κ and ϵ set as in Case 3 defined in Eq. (6).

h	COD_{max}	TCV	#dof
0.0221	0.000513461	0.000432474	43,605
0.0110	0.000499444	0.000406175	100,089
0.0055	0.000489812	0.000391876	176,709
0.0027	0.000484421	0.000384389	628,533
0.0013	0.000481000	0.000380047	2,416,869
Ref. [24]	0.000480000	0.000376991	–

the thickness of the crack and if $\epsilon < h$, the numerical grid could skip the crack. From this error analysis, we propose another setting, where ϵ is smaller in comparison to Case 1 and Case 2 and closer to h while not violating $\epsilon > h$:

$$\textbf{Case3}: \kappa = 10^{-3}h^{0.75} \text{ and } \epsilon = 0.4h^{0.7}. \tag{6}$$

For Conducting the same test series based on the setting in Case 3, the numerical results are given in Fig. 5 and Table 6. Compared to the reference solution given by Sneddon and Lowengrub [24], we achieve very good results for small discretization parameters h.

5. Conclusions

We considered a phase-field fracture model with a focused view on the regularization parameter κ and the length scale ϵ related to Γ-convergence. A proper choice, which satisfies the Γ-convergence conditions while obtaining accurate numerical results, is a challenging task. Error analyses and numerical test runs are conducted on a benchmark test to observe the impact of the considered parameters. The used benchmark test of Sneddon and Lowengrub [14,24] represents a pressure-driven stationary fracture in two dimensions, where exact solutions of certain quantities of interest are available. The best setting for the three relevant parameters is $\kappa = 10^{-3}h^{0.75}$ and $\epsilon = 0.4h^{0.7}$ while $h \to 0$. In this case, we obtain a TCV error of 14.72% and a COD error of 6.97% even for the largest h and the errors reduce to 0.81% (TCV) and 0.2% (COD) on a mesh with around 2.5 million dof. This is a major improvement in comparison to the settings of Case 1 and Case 2 and handles the requirements on ϵ and κ satisfactorily, while not being restricted to a too fine mesh resolution.

It has to be noticed that widely used settings as $\epsilon = 2h$ and κ set sufficiently small, can allow satisfactorily results for a certain application even if Γ-convergence is violated. It means that for $\epsilon \to 0$ we cannot guarantee that the achieved solution is the solution of the energy functional given by Francfort and Marigo [15].

As a future extension, one could investigate the dependency of the parameters on the problem setting and quantities of interest. Even if we are aware of the workload conducting such a detailed error analysis, a more general formula of Case 3 for the relation of κ, h and ϵ could be used by a wider community with interest in reliable simulations of applications based on the theory of Γ-convergence.

Declaration of competing interest

The authors declare that they have no known competing financial interests or personal relationships that could have appeared to influence the work reported in this paper.

References

[1] L. Ambrosio, V.M. Tortorelli, Approximation of functional depending on jumps by elliptic functional via t-convergence, Commun. Pure Appl. Math 43 (8) (1990) 999–1036.
[2] L. Ambrosio, V. Tortorelli, On the approximation of free discontinuity problems, Boll. Unione Mat. Ital. B. 6 (1) (1992) 105–123.
[3] T. Heister, M.F. Wheeler, T. Wick, A primal-dual active set method and predictor-corrector mesh adaptivity for computing fracture propagation using a phase-field approach, Comput. Methods Appl Mech Eng 290 (2015) 466–495.
[4] M.J. Borden, C.V. Verhoosel, M.A. Scott, T.J. Hughes, C.M. Landis, A phase-field description of dynamic brittle fracture, Comput Methods Appl Mech Eng 217 (2012) 77–95.
[5] C. Miehe, F. Welschinger, M. Hofacker, Thermodynamically consistent phase-field models of fracture: variational principles and multi-field FE implementations, Int. J. Numer Methods In Fluids 83 (2010) 1273–1311.
[6] G. Bellettini, A. Coscia, Discrete approximation of a free discontinuity problem, Numer Funct Anal Opt 15 (3–4) (1994) 201–224.
[7] D.B. Mumford, J. Shah, Optimal approximations by piecewise smooth functions and associated variational problems, Commun. Pure Appl Math (1989).
[8] B. Bourdin, Image segmentation with a finite element method, ESAIM: Math Modell Numer Anal 33 (2) (1999) 229–244.
[9] B. Bourdin, G. Francfort, J.-J. Marigo, Numerical experiments in revisited brittle fracture, J. The Mech Phys Solids 48 (2000) 797–826.
[10] M.J. Borden, Isogeometric analysis of phase-field models for dynamic brittle and ductile fracture (Ph.D. thesis), The University of Texas at Austin, 2012.
[11] A. Braides, Approximation Of Free-Discontinuity Problems, in: Lecture notes in Mathematics, (1694) Springer Science & Business Media, 1998.
[12] S. May, J. Vignollet, R. De Borst, A numerical assessment of phase-field models for brittle and cohesive fracture: Γ-convergence and stress oscillations, Eur J Mech-A/Solids 52 (2015) 72–84.
[13] T. Linse, P. Hennig, M. Kästner, R. de Borst, A convergence study of phase-field models for brittle fracture, Eng. Fract. Mech. 184 (2017) 307–318.

[14] J. Schröder, T. Wick, S. Reese, P. Wriggers, R. Müller, S. Kollmannsberger, M. Kästner, A. Schwarz, M. Igelbüscher, N. Viebahn, et al., A selection of benchmark problems in solid mechanics and applied mathematics, Arch. Comput Methods Eng 28 (2) (2021) 713–751.
[15] G. Francfort, J.-J. Marigo, Revisiting brittle fracture as an energy minimization problem, J. The Mech Phys Solids 46 (8) (1998) 1319–1342.
[16] A.A. Griffith, The phenomena of rupture and flow in solids, A, Philos. Trans. R. Soc. Lond. 221 (1921) 229–244.
[17] A. Braides, et al., Gamma-Convergence For Beginners, vol. 22, Clarendon Press, 2002.
[18] G. Dal Maso, An Introduction To Gamma Convergence, Birkhäuser, 1993.
[19] C. Engwer, L. Schumacher, A phase field approach to pressurized fractures using discontinuous Galerkin methods, Math Comput Simul 137 (2017) 266–285.
[20] P.G. Ciarlet, The Finite Element Method For Elliptic Problems, 2. pr., North-Holland, Amsterdam [u.a.], 1987.
[21] T. Heister, T. Wick, Pfm-cracks: A parallel-adaptive framework for phase-field fracture propagation, Software Impacts 6 (2020) 100045.
[22] D. Arndt, W. Bangerth, B. Blais, T.C. Clevenger, M. Fehling, A.V. Grayver, T. Heister, L. Heltai, M. Kronbichler, M. Maier, P. Munch, J.-P. Pelteret, R. Rastak, I. Thomas, B. Turcksin, Z. Wang, D. Wells, The `deal.II` library, version 9.2, J. Numer Math 28 (3) (2020) 131–146.
[23] I.N. Sneddon, The distribution of stress in the neighbourhood of a crack in an elastic solid, Proc. R. Soc. Lond. Ser. A Math. Phys. Eng. Sci. 187 (1946) 229–260.
[24] I.N. Sneddon, M. Lowengrub, Crack Problems In The Classical Theory Of Elasticity, Wiley and Sons, 1969.
[25] T. Wick, Multiphysics Phase-Field Fracture: Modeling, Adaptive Discretizations, and Solvers, 28, Walter de Gruyter GmbH & Co KG, 2020.
[26] M.F. Wheeler, T. Wick, W. Wollner, An augmented-Lagrangian method for the phase-field approach for pressurized fractures, Comput. Methods Appl Mech Eng 271 (2014) 69–85.
[27] T. Heister, T. Wick, Parallel solution, adaptivity, computational convergence, and open-source code of 2d and 3d pressurized phase-field fracture problems, 2018, arXiv:1806.09924.